Journal Pre-proof

Moderate-intensity aerobic exercise training improves $CD8^+$ tumor-infiltrating lymphocytes effector function by reducing mitochondrial loss.

Vanessa Azevedo Voltarelli, Mariane Tami Amano, Gabriel Cardial Tobias, Gabriela Silva Borges, Ailma Oliveira da Paixão, Marcelo Gomes Pereira, Niels Olsen Saraiva Câmara, Waldir Caldeira, Alberto Freitas Ribeiro, Leo Edmond Otterbein, Carlos Eduardo Negrão, James Turner, Patricia Chakur Brum, Anamaria Aranha Camargo

PII: S2589-0042(24)01346-4

DOI: https://doi.org/10.1016/j.isci.2024.110121

Reference: ISCI 110121

To appear in: ISCIENCE

Received Date: 17 October 2023

Revised Date: 9 February 2024

Accepted Date: 24 May 2024

Please cite this article as: Voltarelli, V.A., Amano, M.T., Tobias, G.C., Borges, G.S., Oliveira da Paixão, A., Pereira, M.G., Saraiva Câmara, N.O., Caldeira, W., Ribeiro, A.F., Otterbein, L.E., Negrão, C.E.,

Turner, J., Brum, P.C., Camargo, A.A., Moderate-intensity aerobic exercise training improves $CD8^+$ tumor-infiltrating lymphocytes effector function by reducing mitochondrial loss., *ISCIENCE* (2024), doi: https://doi.org/10.1016/j.isci.2024.110121.

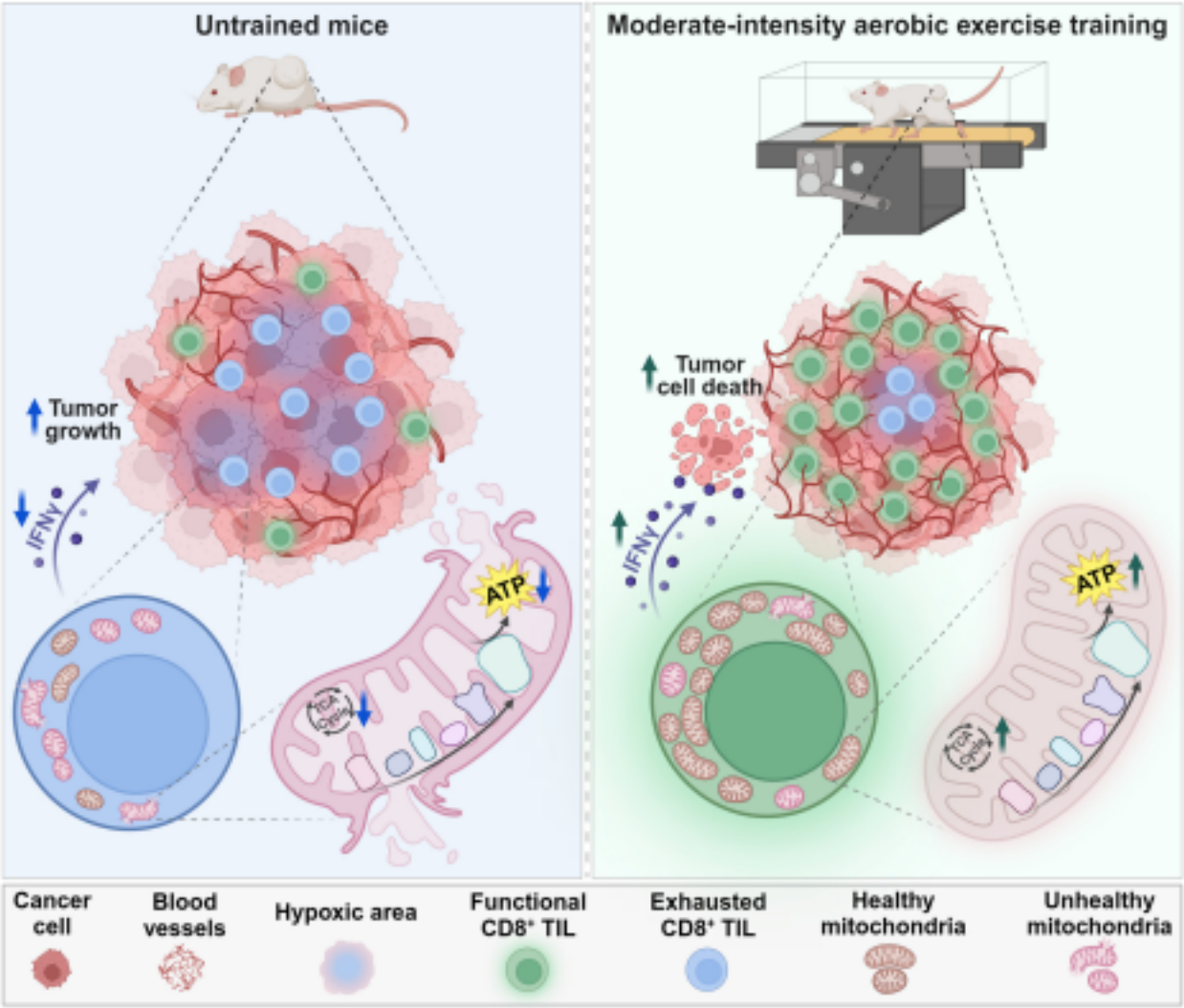

Article

Moderate-intensity aerobic exercise training improves CD8$^+$ tumor-infiltrating lymphocytes effector function by reducing mitochondrial loss.

Vanessa Azevedo Voltarelli* [1,2,3]; Mariane Tami Amano [1]; Gabriel Cardial Tobias [2,4] 6 ;Gabriela Silva Borges [2]; Ailma Oliveira da Paixão [2]; Marcelo Gomes Pereira [2,5]; Niels Olsen Saraiva Câmara [6] 7 ;

Waldir Caldeira [7]; Alberto Freitas Ribeiro [7]; Leo Edmond Otterbein [3]; Carlos Eduardo Negrão [2,8] 8 ; James Turner [9,10]; Patricia Chakur Brum[ϛ 2,11]; Anamaria Aranha Camargo[ϛ 1] 9 . 10
11
12 1. Molecular Oncology Center, Sírio-Libanês Hospital, São Paulo, SP, Brazil.
13 2. School of Physical Education and Sport, University of São Paulo, SP, Brazil. 14 3. Department of Surgery, Beth Israel Deaconess Medical Center, Harvard Medical School, Boston, MA, 15 USA.
16 4. Department of Pediatrics, Weill Cornell Medical College, New York, NY, USA. 17 5. Leeds School of Biomedical Sciences, Faculty of Biological Sciences, University of Leeds, UK. 18 6. Department of Immunology, Institute of Biomedical Sciences, University of São Paulo, SP, Brazil. 19 7. Department of Genetics and Evolutionary Biology, University of São Paulo, SP, Brazil. 20 8. Heart Institute, Faculty of Medicine, University of São Paulo, SP, Brazil
21 9. Department for Health, University of Bath, Bath, UK.
22 10. School of Sport, Exercise and Rehabilitation Sciences, University of Birmingham, UK 23 11. Department of Physiology & Biophysics, Institute of Biomedical Sciences, University of São Paulo, SP, 24 Brazil.
252627
28
29 ϛ ***Equal contribution of senior authors***
303132
33 * **Corresponding and Lead author:**
34 Vanessa Azevedo Voltarelli, PhD.
35 Harvard Medical School
36 Beth Israel Deaconess Medical Center, Center for Life Sciences, CLS 603
37 3 Blackfan Street, Boston, MA 02115 - USA
38 Phone: (+1) (617) 735-2851
39 E-mail: vvoltare@bidmc.harvard.edu

40 **SUMMARY**

41 Aerobic exercise training (AET) has emerged as a strategy to reduce cancer mortality, however 42 the mechanisms explaining AET on tumor development remain unclear. Tumors escape immune 43

detection by generating immunosuppressive microenvironments and impaired T cell function, 44 which is associated with T cell mitochondrial loss. AET improves mitochondrial content and 45 function, thus we tested whether AET would modulate mitochondrial metabolism in tumor
46 infiltrating lymphocytes (TIL). Balb/c mice were subjected to a treadmill AET protocol prior to CT26
47 colon carcinoma cells injection and until tumor harvest. Tissue hypoxia, TIL infiltration and effector
48 function, and mitochondrial content, morphology and function were evaluated. AET reduced tumor

growth, improved survival, and decreased tumor hypoxia. An increased $CD8^+$ 49 TIL infiltration, IFN 50
γ and ATP production promoted by AET was correlated with reduced mitochondrial loss in these cells.
Collectively, AET decreases tumor growth partially by increasing $CD8^+$ 51 TIL effector function 52
through an improvement in their mitochondrial content and function.
53
54
55
56
57
58
59
60
61
62
63
64
65
66
67
68
69
70
71

INTRODUCTION

In 2018, the national expenditure for cancer care in the United States was estimated at $150.8 billion. Costs are likely to increase due to increases in lifespan and the adoption of new and more expensive treatments, such as checkpoint inhibitor immunotherapy[1,2]. Therefore, a better understanding of factors and environmental conditions that can prevent or decrease cancer incidence and mortality would be of great value. Aerobic exercise training (AET) reduces the incidence and mortality of several cancer types[3–10]. In 2016, Moore and collaborators showed that among 1.44 million adults from USA and Europe, high levels of leisure-time physical activity were positively correlated with a significant reduction in the incidence of 13 types of cancer[11].

Furthermore, the World Cancer Research Fund (WCRF) points out that moderate physical activity (such as brisk walking) as well as vigorous physical activity (including running, fast cycling and aerobics) decreases the risk of colon, womb and post-menopausal breast cancer[12]. Previous clinical findings also indicated that cancer patients with reduced aerobic capacity present a poorer prognosis of the disease[13–16].

While epidemiological studies indicate that high levels of physical activity in general reduce the risk of cancer development, it is likely that the anti-cancer mechanisms are most robustly stimulated by structured and long-term moderate-to-vigorous intensity AET[17]. However, these molecular mechanisms underlying the benefits of AET on cancer incidence and mortality are still poorly understood. There is an increasing number of studies addressing this question that provide new insights into potential mechanisms of action by which exercise reduces tumor growth and progression, including the modulation of systemic and intratumoral immunity[18–20]. Tumors escape initial immune detection by generating an immunosuppressive intratumoral microenvironment which limits immune cell infiltration, activation, and effector function. Recent studies have shown that exercise can modulate immune cell mobilization and anti-tumor immunity[21]. For example, Rundqvist and collaborators using a mouse model of breast cancer showed that voluntary exercise-mediated reduction in tumor growth is dependent on cytotoxic $CD8^+$ T cell infiltration, and that skeletal muscle metabolites released during high intensity exercise into plasma enhances $CD8^+$ T cell effector function[19]. Others have also demonstrated that exercise enhances $CD8^+$ T

cell infiltration and effector function and improves responses to checkpoint inhibitors immunotherapy[22]
103 .
104 Mitochondrial dynamics and metabolism have been identified as key modulators of TIL fate and effector function[23–25] 105 . Impaired TIL effector function has been associated with a persistent 106 loss of mitochondrial content and function, which is directly associated with a decrease in 107 interferon-gamma (IFN-γ) production. Additionally, impaired TIL effector function was shown to
108 be tumor microenvironment specific, and largely independent of PD-1 blockade or regulatory T cell suppression[24]. Also, mitochondrial dysfunction in $CD8^+$ 109 TIL has been shown to reinforce phenotypic and epigenetic reprograming for T exhaustion[25] 110 .
111 AET improves aerobic fitness and metabolism, which occurs primarily through significant increases in mitochondria number, volume and function in different body tissues [26] 112 . Therefore, in 113 the present study we tested the hypothesis that AET would modulate TIL mitochondrial content, 114 function, and morphology, thereby preventing or mitigating impairment of their effector function. 115 The key findings of our study are that moderate-intensity AET improves survival and morbidity 116 while reducing tumor growth in the CT26 animal model of colorectal cancer. These outcomes

were associated with an increase in both the number and effector function of $CD8^+$ 117 TILs. We also found that AET prevents the loss of $CD8^+$ 118 TIL mitochondrial density and function, and that this is associated with an improved effector/cytotoxic $CD8^+$ 119 TIL function.
120

121 **RESULTS**

122 **Aerobic exercise training increases survival and reduces morbidity in a colorectal cancer 123 mice model.** The experimental design of the study is shown in **Figure 1A**. Moderate-intensity 124 AET performed prior to tumor cell inoculation and continued during tumor development improved 125 overall survival in tumor-bearing trained mice (CT26 TR) compared to tumor-bearing sedentary 126 mice (CT26 SED) (**Figure 1B**). CT26 TR mice also showed a less pronounced body weight loss 127 and improved aerobic capacity at day 13 after tumor cell inoculation compared to CT26 SED 128 group (46% vs. 69% drop in total distance, $p<0.01$), (**Figures 1C-D**). CT26 TR mice exhibited a 129 decrease in epididymal fat mass but no significant difference in tibialis, soleus and gastrocnemius 130 muscles masses compared to CT26 SED mice (**Figure S1A-D**). These data indicate that AET 131 attenuates

cancer-related morbidity while improving survival.

Aerobic exercise training reduces tumor latency, growth and hypoxic core and increases immune cell tumor infiltration. CT26 TR mice showed a delay in tumor latency compared to CT26 SED group as assessed by the detection of palpable tumors (**Figure 2A**). Also, moderate intensity AET significantly decreased tumor growth measured over 13 days post-inoculation (**Figures 2A-B**). The greatest difference in tumor growth and ex-vivo mass was observed at day 9 (**Figures 2C-E**) and thus, all further analyses were performed on tumors harvested on day 9 post-inoculation, since we considered this time point as the one with maximum effect of AET on tumor growth. Interestingly, we observed a significant negative correlation between aerobic capacity evaluated before tumor cell inoculation and tumor volume measured at day 9, indicating that improved aerobic capacity has a quantitative effect on tumor growth. (**Figure 2F**). In addition to the effects on tumor growth, AET significantly reduced the percentage of hypoxic areas within the tumor microenvironment (TME) of CT26 TR mice compared to CT26 SED mice (**Figures 3A C**), which was accompanied by an increase in the number of infiltrating immune cells (**Figures 3D-E**).

Aerobic exercise training modulates the composition and function of TILs. In parallel with an increased number of immune cells infiltrating the TME, we observed that AET specifically increases the total number of tumor-infiltrating T cells when compared to CT26 SED (**Figures 4A**

D). When distinguishing TIL by their subpopulations, we observed that the population of $CD4^+$ T cells did not statistically differ among the CT26 SED and CT26 TR groups (**Figure 4E**), while the number of regulatory T cells (Treg) showed a significant decrease in CT26 TR in comparison to CT26 SED mice (**Figure 4F**). The decreased percentage of Treg cells in tumors of trained mice supports the significant increase in the population of $CD8^+$ T cells in the CT26 TR group, which was accompanied by a significant increase in the percentage of activated $CD8^+$ T cells when compared to CT26 SED mice (**Figures 5A-B**). In accordance, CT26 TR mice showed a higher population of $CD8^+$ T cells in the draining lymph nodes (dLN) compared to CT26 SED mice (**Figure S2C**).

$CD8^+$ TIL function was also evaluated by measuring interferon gamma (IFNγ), since this cytokine is

critical for T cell effector function against tumor cells[27] 161 . AET significantly increased the percentage of IFNγ$^+$ CD8$^+$ 162 T cells in tumors of CT26 TR compared to CT26 SED (**Figure 5C-D**), indicating that CD8$^+$ 163 TILs from CT26 TR mice are more capable of producing IFNγ and potentially 164 killing tumor cells. However, there were no statistically significant differences between groups for CD8$^+$ TIL populations positively expressing the checkpoint receptor PD-1$^+$ 165 (**Figure 5E**), indicating 166 that this mechanism is not associated with reduced tumor growth and with increased infiltration 167 of effector T cells induced by AET.

168

Aerobic exercise training prevents loss of CD8$^+$ 169 **TIL mitochondrial content and function,** 170 **which is associated with increased IFNγ production.** It has been shown that morphological 171 changes in mitochondria, controlled by the balance between mitochondrial fusion and fission, are 172 a primary signal that shapes metabolic reprogramming during T cell quiescence and activation[23,25]. Therefore, electron microscopy images of CD8$^+$ 173 TIL isolated from CT26 SED and 174 CT26 TR mice were analyzed but showed no significant differences between groups for the 175 different mitochondrial morphology parameters evaluated (mitochondrial area, elongation, and circularity). The only significant difference observed was that CD8$^+$ 176 TILs from CT26 TR exhibited 177 an increased number of mitochondria when compared to TILs from CT26 SED mice (**Figures 6A E**). Corroborating these data, CT26 TR CD8$^+$ 178 TIL exhibited a significant increase in mitochondrial 179 density evaluated by MitoTracker Green when compared to TILs from CT26 SED mice (**Figure 6F**). Interestingly, when CD8$^+$ 180 TIL mitochondrial densities of tumor-bearing mice were compared 181 to the mitochondrial density of T cells isolated from inguinal lymph nodes of healthy sedentary 182 control mice, we observed that both CT26 SED and CT26 TR lymphocytes infiltrating the TME 183 lost a significant amount of mitochondrial content. Even though AET was unable to bring TILs mitochondrial content to control levels, CD8$^+$ 184 TIL loss of mitochondrial density in CT26 TR mice

185 was partially prevented when compared to CT26 SED (**Figure 6G**). We also showed that the total 186 TILs from CT26 TR exhibit an increase in protein expression of mitochondrial complex III when 187 compared to CT26 SED mice, with no significant changes in mitochondrial complexes I, II and IV 188 expressions (**Figure S2E**). However, the total TILs protein expression of dynamin-like GTPase Mitofusin 1 (Mfn1), essential for mitochondrial fusion[28] 189 , was not different between the groups 190 (**Figure S3A**). In addition, no significant differences were observed in the gene expression of PINK1,

PARK2, ULK1, BNIP3, ATG5, ATG7, and LC3B, markers of autophagy/mitophagy[29,30] 191 , in 192 the solid tumors of CT26 TR compared to CT26 SED mice (**Figure S3B-H**).

As can be seen in **Figures 6H-I**, the partial increase in $CD8^+$ 193 TILs mitochondrial density by 194 AET was associated with an increased number of healthy/functional mitochondria in these cells, since $CD8^+$ 195 TIL from CT26 TR showed a higher mitochondrial membrane potential (ΔΨM), 196 represented by the red/green fluorescence ratio (healthy/unhealthy mitochondria), when 197 compared to TIL from CT26 SED mice. In addition, AET significantly increased the ATP 198 production of the total tumor-infiltrating immune cells compared to sedentary controls, suggesting 199 that AET not only induces an increase in mitochondrial content, but also improves their oxidative 200 phosphorylation (OXPHOS) function (**Figure 6J**). Indeed, an *in-silico* analysis of a public microarray dataset (Geo Dataset GSE68072[31] 201) comparing peripheral blood leukocytes in young 202 endurance athletes (outside the competition period) to non-athletes at rest, showed that the 203 leukocytes of athletes present an increase in expression of OXPHOS genes compared to non 204 athletes (**Figure S2D**).

205 To determine if there is a direct and positive association between mitochondrial 206 content/function and the T cell effector function, leukocytes were isolated from draining lymph 207 nodes (inguinal) of CT26 SED and CT26 TR animals. The cells were treated with oligomycin (a 208 mitochondrial ATP synthase inhibitor), and FCCP (a mitochondrial uncoupler, widely used for assessing maximal oxygen consumption by mitochondria). We observed that $CD8^+$ 209 T cells 210 isolated from CT26 TR mice showed an increase in IFNγ production compared to CT26 SED mice 211 when maximal mitochondrial function was induced with FCCP. No significant differences were 212 observed between the groups for the baseline and the oligomycin conditions (**Figures 6K-L**). 213 These data suggests that the enhanced oxidative metabolism promoted by AET can lead to increased effector function of $CD8^+$ 214 T cells in tumor-bearing mice, which may partially contribute 215 to the observed decreased tumor growth in CT26 TR compared to CT26 SED mice.

216

217 **DISCUSSION**

218 The principal findings of the present study were that AET inhibited tumor growth and limited 219 the hypoxic area of the TME, which correlated with an increase in both the number and effector function of $CD8^+$ TILs. In addition, in sedentary mice, $CD8^+$ 220 TILs exhibited reduced mitochondrial content and

function, which was prevented in part by AET. Finally, $CD8^+$ 221 T cells from AET mice 222 exhibited elevated IFNγ, which was accompanied by induction of maximal mitochondrial function, supporting a cause-and-effect relationship between improved $CD8^+$ 223 T cell mitochondrial 224 bioenergetics and effector functionality.

225 The beneficial effects of AET in reducing cancer incidence and the tumor growth have been extensively shown [8,20,32–34] 226 . Here we corroborate those findings using a colorectal cancer animal 227 model, in which a moderate-intensity AET protocol performed before and after tumor cells 228 inoculation significantly decreased tumor growth while increasing the survival rate and reducing 229 morbidity. In support, Lakoski and collaborators showed in 2015 that lung and colon cancer 230 patients with greater physical capacity exhibited longer survival rates compared to patients with less physical capacity[35] 231 . It had also been demonstrated that colon cancer patients present a 232 reduction, greater than 20%, in their maximum oxygen consumption ($VO_{2\ max}$) compared to their healthy peers, which is followed by reduced lean mass measured in their legs[14] 233 . Considering that, 234 AET is known to attenuate the loss of body and skeletal muscle masses, which is usually triggered by pro-cachectic types of cancer, such as colon cancer [36,37] 235 . Encouragingly, our data show that 236 AET can prevent the loss of body mass, associated with an attenuated loss of aerobic capacity 237 that was induced by cancer progression. It is important to highlight, however, that a recent study 238 has shown that exercise worsened survival in colorectal tumor-bearing mice when performed in association with chemotherapy in late stages of cachexia[38] 239 .

240 Our findings can be partially explained by the effects of AET on the TME at a cellular level. We here propose, based on previous studies in the literature[32,39,40] 241 , that AET increases tumor 242 perfusion through an improved functional angiogenesis, which facilitate the infiltration of immune 243 cells in the TME, as seen in **Figures 3D-E**. The increased number of functional blood vessels

244 irrigating the TME induced by the AET will further reduce the TME hypoxic areas, as shown in **Figures 3B-C.** The reduced area of hypoxia, in turn, improves the effector function of $CD8^+$ 245 T 246 cells by preventing their loss of mitochondrial content and activity. In fact, it has been previously 247 shown that dysfunctional vascularization and its consequent hypoxic areas can lead to metabolic exhaustion of immune cells infiltrating the TME[39–41] 248 .

In support, our data show that AET increases the number of activated $CD8^+$ 249 TIL populations, which exhibit increased IFNγ production. The improved $CD8^+$ 250 TIL function induced by AET may 251 also be partially related to the reduced population of Treg cells in the TME, since these are known to suppress the cytotoxic function of immune cells[42] 252 .

253 Improvements in metabolic control is another important factor to be considered as being partially responsible for increased $CD8^+$ 254 TIL effector function in trained mice. Since activated T cells depend on aerobic glycolysis to produce ATP[43] 255 , the mitochondria function plays an essential 256 role on T cells, besides being historically neglected in the literature. However, mitochondria 257 cannot just be seen as an ATP source, considering that these organelles are also involved in calcium homeostasis, lipid synthesis, apoptosis, signaling, and cell cycle progression[44] 258 . In fact, 259 mitochondrial metabolism has been shown to play a key role in the differentiation and in fate of T cells[25,45] 260 . Although there is evidence demonstrating that an increased OXPHOS reduces IFNγ secretion by T cells[46] 261 , it has recently been shown that, during their first hours of activation, T cells dramatically increase mitochondrial mass, as well as mitochondrial DNA levels[46] 262 , and that this mitochondrial biogenesis induction is indispensable for them to escape quiescence[47] 263 . This 264 evidence corroborates our results that show a positive and direct effect of the maximal mitochondrial function on IFNγ production by $CD8^+$ 265 T cells, associated with an attenuated loss of 266 mitochondrial density in TIL by the AET. A significant increase in ATP production and in the 267 mitochondrial complex III expression in tumor-infiltrating leukocytes were also promoted by AET 268 (**Figure S2**). It is important to highlight that complex III is an important reactive oxygen species 269 (ROS) source in mitochondria, and that mitochondrial ROS production is important for T cell activation[43,48] 270 . Moreover, T cells that do not express the complex III subunit Uqcrfs1, necessary 271 to produce mitochondrial ROS, are not able to produce IL-2, a cytokine that is essential for 272 maturation and proliferation. Besides being a well-accepted index of mitochondrial health and functionality[23,25], $CD8^+$ 273 TIL mitochondria morphology was not changed by AET, even though a 274 significant increase in the ΔΨM was seen in these cells when compared to the sedentary group. 275 Additionally, the morphology data indicates that the increased mitochondrial number showed in the $CD8^+$ 276 TIL from trained mice cannot be explained by the process of mitochondrial fission.

277 The discovery of new mechanisms associated with a reduced tumor growth promoted by the 278 AET might support the future development of pharmacological and non-pharmacological 279 therapies for treating cancer. In this regard, it is relevant to highlight that metformin, an approved 280 medication used in patients with diabetes, has been pointed as a potential drug in oncology clinic, 281 since observational studies reported decreased cancer incidence and cancer-related mortality among people taking this medication[49,50] 282 . The mechanisms of action of its anticancer properties 283 are still under

investigation, but one strong candidate is the activation of AMP-activated protein 284 kinase (AMPK), an energy sensor that regulates cellular and mitochondrial metabolism and which is well known to be highly activated by aerobic exercise[51] 285 . Accordingly, activators of AMPK, such

286 as AICAR (5-Aminoimidazole-4-carboxamide ribonucleoside), are currently some of the most effective exercise mimetics emerging as therapeutic targets[52,53] 287 . Moreover, as muscle-derived 288 myokines that are released during exercise (e.g., IL-6 and IL-15) have been shown to regulate the TME and its infiltrating immune cells[54,55] 289 , future studies are needed to better understand 290 muscle-tumor crosstalk within the context of AET and its potential clinical utility in the treatment 291 of cancer. Therefore, the use of exercise mimetics in oncology, and the formal inclusion of 292 exercise training protocols for cancer patients as adjuvant therapies should be encouraged as 293 more scientific evidence accumulates.

294 Taken together, we provide evidence that a structured moderate intensity AET, performed 295 before and after tumor establishment, increases survival rate and decreases morbidity and tumor growth through the modulation of $CD8^+$ 296 TIL effector function and their mitochondrial content and 297 function in a mouse model of colorectal cancer. Altogether, we provide new insights on the 298 molecular and immunological mechanisms whereby AET controls tumor growth and progression. 299

300 **Limitations of the study**

301 While we presented evidence of a potential new mechanism by which aerobic exercise training (AET) may modulate the metabolism and function of $CD8^+$ 302 tumor-infiltrating lymphocytes 303 (TILs), it's important to acknowledge several limitations in our study. Our hypothesis was tested 304 only in a heterotopic colorectal cancer model, implying that the reported findings might not 305 generalize across other cancer types or even orthotopic colorectal models subjected to AET. 306 Moreover, based on the data presented, we cannot definitively conclude that the observed effects of AET on $CD8^+$ 307 TILs mitochondrial density and effector function are entirely direct, as they may 308 be influenced by other tumor microenvironment (TME) components also modulated by exercise, such as angiogenesis, innervation, tumor cell metabolism, and various immune cell types[56] 309 .

Another limitation lies in our analysis of the isolated mitochondrial morphology of $CD8^+$ 310 TILs, 311 as the T cell purification process from digested tumors could potentially induce significant changes in mitochondrial dynamics and function. Ideally, the evaluation of gold-labeled $CD8^+$ 312 T cell 313 mitochondria content in tumors fixed for electron microscopy immediately after harvest would 314

provide more accurate insights.

Therefore, these limitations highlight the need for further investigation into the effects of AET on $CD8^+$ TILs mitochondrial metabolism in the field of cancer research. Additional studies are needed to corroborate and supplement our findings, as well as those of other studies in the literature of cancer and exercise.

ACKNOWLEDGMENTS

The authors want to thank Fundação de Amparo à Pesquisa do Estado de São Paulo for the financial support (FAPESP, 2015/22814-5, and 2017/13133-0).

AUTHOR CONTRIBUTIONS

Conceptualization: VAV, MTA, GCT, PCB, and AAC; intellectual contribution: VAV, MTA, GCT, JT, PCB, and AAC; methodology and data acquisition: VAV, MTA, GSB, AOP, MGP, NOSC, WC, and AFR; formal analysis: VAV; resources: CEN, JT, PCB, and AAC; writing—original draft preparation: VAV and LEO; writing—review and editing: VAV, MTA, GCT, LEO, JT, AAC, and PCB; supervision: PCB and AAC. All authors have read and agreed to the published version of the manuscript.

DECLARATION OF INTERESTS

No competing interests, financial or otherwise, are declared by the author(s).

FIGURE LEGENDS

Figure 1. Moderate-intensity aerobic exercise training increases survival and aerobic capacity in mice with colorectal cancer. (**A**) Study experimental design, (**B**) survival rates, (**C**) body mass changes post-tumor cell inoculation, and (**D**) aerobic capacity represented as distance run in meters during an exhaustion test on day 13 after tumor cell inoculation, comparing sedentary animals (Control), sedentary tumor-bearing mice (CT26 SED), and trained tumor bearing mice (CT26 TR). Data represent mean ± SEM. Comparison of survival curves by Log rank (Mantel-Cox) test (*p=0.0356). Repeated measures ANOVA, and One-way ANOVA, followed

by Duncan's post hoc. *p<0.05, **p<0.01 vs. control, and #p<0.05 vs. CT26 SED.

Figure 2. Moderate-intensity aerobic exercise training decreases CT26 tumor growth in mice with colorectal. (**A**) Tumor latency, (**B**) tumor volume measured for 13 days following CT26 cells inoculation; arrow indicates the time with the largest statistical difference between groups (9 days), (**C**) tumor volume measured up to day 9 after tumor cell inoculation, (**D**) *ex vivo* tumor mass at day 9, (**E**) representative images of *ex vivo* solid tumors at day 9, and (**F**) correlation between aerobic capacity evaluated after AET and before CT26 inoculation and tumor volume measured at day 9 comparing sedentary tumor-bearing mice (CT26 SED) and trained tumor bearing mice (CT26 TR). Data represent mean ± SEM. Tumor latency curves by Log-rank (Mantel-Cox) test (**p=0.0039). Unpaired Student's *t* test. #p<0.05, ##p<0.01, ###p<0.001, and ####p<0.0001 vs. CT26 SED.

Figure 3. Aerobic exercise training decreases tumor hypoxia while increasing total tumor infiltrating immune cells. (**A**) Experimental protocol, (**B**) tumor hypoxic area quantitatively measured by fluorescence, (**C**) immunohistological images (100x) of tumor sections stained with DAPI (nuclear), a pimonidazole primary antibody (Hypoxyprobe), followed by a FITC-secondary antibody incubation, and (**D-E**) total tumor-infiltrating leukocytes percentage ($CD45^+$) analyzed by flow cytometry comparing sedentary tumor-bearing mice (CT26 SED) and trained tumor-bearing mice (CT26 TR) at day 9 post-tumor cell inoculation. Data represent mean ± SEM. Unpaired Student's *t* test. #p<0.05 vs. CT26 SED.

Figure 4. Tumor-infiltrating T cell populations are modulated by aerobic exercise training. (**A-B**) Tumor-infiltrating T cells evaluated in tumor histological sections stained with hematoxylin eosin (200x), (**C-D**) total TILs ($CD3^+$) evaluated by flow cytometry, (**E**) total tumor-infiltrating $CD4^+$ T cells, and (**F**) regulatory T cells (Treg), comparing sedentary tumor-bearing mice (CT26 SED) and trained tumor-bearing mice (CT26 TR). Data represent mean ± SEM. Unpaired Student's *t* test. #p<0.05 vs. CT26 SED.

Figure 5. Aerobic exercise training increases the number and function of $CD8^+$ tumor

infiltrating T cells. (**A-B**) Total and activated tumor-infiltrating $CD8^+$ 372 T cells, and the populations of (**C-D**) IFN-γ^+ and (**E**) PD-1^+ $CD8^+$ 373 TILs, comparing sedentary tumor-bearing mice (CT26 SED) 374 and trained tumor-bearing mice (CT26 TR). Data represent mean ± SEM. Unpaired Student's *t* 375 test. #p<0.05 vs. CT26 SED.

376

Figure 6. Increased IFNγ production in $CD8^+$ 377 **TILs promoted by aerobic exercise training is** 378 **associated with improved mitochondrial density and function.** (**A**) Mitochondrial number per cell, (**B-D**) area, elongation, and circularity of $CD8^+$ 379 TILs isolated using magnetic beads, and (**E**) representative transmission electron microscopy images, (**F**) $CD8^+$ 380 TILs mitochondrial density 381 evaluated by the MitoTracker Green fluorescent probe, (**G**) and compared to the mitochondrial density of inguinal lymph node $CD8^+$ 382 T cells harvested from healthy sedentary controls (white bars), (**H-I**) the ratio between $CD8^+$ 383 TILs with high and low mitochondrial membrane potential 384 (healthy and unhealthy mitochondria, respectively) evaluated by the JC-1 fluorescent probe, and 385 (**J**) ATP production by total tumor-infiltrating leukocytes comparing sedentary tumor-bearing mice

386 (CT26 SED) and trained tumor-bearing mice (CT26 TR). (**K-L**) Production of IFNγ (median fluorescence intensity, MFI) by draining lymph node (dLN) $CD8^+$ 387 T cells under baseline condition, 388 and in response to oligomycin (mitochondrial ATP synthase inhibitor) and FCCP (inducer of 389 maximal oxygen consumption by mitochondria), comparing sedentary animals (Control), 390 sedentary tumor-bearing mice (CT26 SED), and trained tumor-bearing mice (CT26 TR). Data 391 represent mean ± SEM. Unpaired Student's *t* test, and One-way ANOVA, followed by Duncan's 392 post hoc. **p<0.01, ***p<0.001 vs. control, and #p<0.05 vs. CT26 SED.

393

394 **STAR METHODS**

395

396 **KEY RESOURCES TABLE** (Separate Word file)

397

398 **RESOURCE AVAILABILITY**

399 **Lead contact**

400 Any additional information and requests for resources and reagents should be directed to and 401

will be fulfilled by the lead contact, Vanessa A. Voltarelli (vvoltare@bidmc.harvard.edu).

Materials availability

This study did not generate new unique reagents.

Data and code availability

• This paper does not report original code.

• Data sets have been deposited at Mendeley. The DOI is listed in the key resources table. Microscopy data reported in this paper will be shared by the lead contact upon request.

• Any additional information required to reanalyze the data reported in this work is available from the lead contact upon request.

EXPERIMENTAL MODEL AND STUDY PARTICIPANT DETAILS

Animal model. Male Balb/c mice (8 weeks old) were housed in the animal facility of the School of Physical Education and Sport at University of Sao Paulo, in a temperature-controlled environment (22°C) and in a reversed 12:12-h dark-light cycle. Standard laboratory chow (Nuvital Nutrients, Curitiba, Brazil) and tap water were available ad libitum. The sample size for each

experiment is indicated in the figures. Euthanasia was performed by cervical dislocation under isoflurane anesthesia (3.5%, administered in medical air enriched with oxygen). All procedures were in accordance with the Guide for the Care and Use of Laboratory Animals (National Institutes of Health, Bethesda, MD, USA) and with ethical principles in animal research adopted by the Brazilian Council for the Control of Animal Experimentation (CONCEA). In addition, this study was approved by the Ethical Committee of the School of Physical Education and Sport, University of Sao Paulo (protocol # 2017/02).

Running capacity test and aerobic exercise protocol. Aerobic exercise capacity was evaluated using a graded treadmill exercise test for mice previously standardized by our research group[57] . Mice were acclimatized to the treadmill for a week before the running capacity test (10 minutes of exercise/session in low speed). On the day of the test, each mouse was placed in

individual treadmill lanes (Treadmill for Multiple Rodents, Grupo AVS – AVS Projetos, Sao Carlos, 431 Brazil) and allowed to acclimatize for 5 minutes. After that, intensity of exercise was increased by 432 3 m/min (starting at 6 m/min) every 3 min until exhaustion. Exhaustion was defined as the moment 433 when animals were unable to keep pace with the treadmill for up to 1 minute. Mice were then 434 randomized into sedentary and training groups based on the maximal velocity (Vmax) achieved 435 in the incremental maximal test, ensuring that both groups exhibited similar average Vmax values 436 with no significant statistical difference between them. Moderate-intensity aerobic exercise 437 training (AET) sessions were performed at 60% of the mean Vmax, for 1 hour/day, 5 days/week, 438 for 30 days before tumor cells inoculation. Mice were kept under the same AET protocol for 9 or 439 13 days after tumor cells inoculation.

440

441 **CT26 colon carcinoma cell line.** CT26 cells were cultured in RPMI 1640 Medium supplemented 442 with 10% Fetal Bovine Serum, 1X Penicillin-Streptomycin, at 37ºC and 5% CO_2, and were regularly tested for Mycoplasma contamination. $1x10^6$ 443 resuspended cells (in 100 µL of PBS) were

444 inoculated subcutaneously in the upper flank 48 hours after the last exercise session of the fourth 445 week of AET. Evaluation of tumor growth was performed daily after tumor cell inoculation using a 446 digital caliper. The largest and smallest tumor diameters were measured, and values obtained 447 were used to calculate tumor volume using the following formula: V = 0.52 x (largest diameter) x (smallest diameter)^2 448 .

449

450 **METHOD DETAILS**

451 **Tumor histology.** Solid tumors harvested 9 days after tumor cell inoculation were fixed in 4% 452 paraformaldehyde (PFA) and embedded in paraffin for further staining with hematoxylin and eosin

453 (H&E) using a standard protocol. H&E images were captured at 200X magnification. The number 454 of tumor-infiltrating lymphocytes was evaluated using ImageJ's automatic particle counting tool. 455 Five tumors per group were analyzed, with an average of 18 images per tumor. The quantitative data were expressed in number of particles/cells per area (µm^2 456).

457 For the assessment of tumor hypoxia, the Hypoxyprobe Kit was used. Animals received an 458 intraperitoneal injection of pimonidazole HCl (60 mg/kg) 30 minutes before euthanasia. After 459

harvesting, solid tumors were embedded in the cryoprotectant Tissue-Tek® O.C.T., frozen in dry 460 ice, and stored at -80°C until sectioning. Upon thawing, tumor sections (5 μm) were fixed in cold 461 acetone (4°C) for 10 minutes and incubated overnight at 4°C with anti-pimonidazole antibody 462 (1:50, diluted in PBS containing 0.1% bovine serum albumin and 0.1% Tween 20). Subsequently, 463 the sections were incubated for 1 hour at room temperature with Alexa Fluor™ 488-conjugated 464 secondary antibody (1:300). Slides were mounted using a mounting medium with DAPI for 465 nucleus staining. Images were captured at 100X magnification. The area of tumor hypoxia was 466 assessed by ImageJ (). Five tumors per group were analyzed, with an average of 10 images per 467 tumor. The quantitative data were expressed in integrated density (fluorescence) corrected per 468 area analyzed.
469
470 **Tumor digestion.** Tumors were cut into small pieces and further digested in 1X PBS containing 471 2% of Fetal Bovine Serum (FBS), collagenase type IV (2 mg/mL), and DNAse I (5U/mL), for 40 472 minutes at 37°C, with 150 rpm agitation. After digestion, the cell homogenate was filtered in 70 473 μm cell strainers and subjected to a Percoll gradient to obtain an enriched fraction of immune 474 cells (total leukocytes). Inguinal draining lymph nodes (dLN) were mechanically homogenized in 475 70 μm cell strainers with 1X PBS supplemented with 2% of FBS to obtain an immune cells 476 suspension.
477
478 **Flow cytometry.** Total immune cells isolated from digested tumors and dLN were first incubated 479 with TruStain FcX™ antibody (1:100) for 10 minutes at 4°C to block nonspecific binding of 480 immunoglobulin to the Fc receptors. Subsequently, the samples were incubated with 481 fluorochrome-conjugated antibodies: FVS (Fixable Viability Stain Reagent), CD45, CD3, CD4, 482 CD8, CD25, FOXP3, PD-1, and IFN-γ (1:40 dilution) for 30 minutes at 4°C. A list of the antibodies 483 used can be found in the key resources table. Following staining, the samples were fixed with BD 484 Fixation/Permeabilization Solution for 20 minutes at 4°C. Intracellular staining for FOXP3 was 485 conducted after fixing and permeabilizing the cells using the BD Mouse Foxp3 Buffer Set. For the 486 evaluation of IFN-γ production, a portion of the isolated cells was stimulated for 6 hours in culture

487 (37°C and 5% CO_2) with phorbol 12-myristate 13-acetate (PMA, 0.02 μg/mL) plus ionomycin (1 μg/mL), under Golgi blockade, before antibody incubation[58] 488 . The cells were also stained with the 489 fluorescent probes MitoTracker ™ Green FM and JC-1 for mitochondrial density and membrane

490 potential assessment, respectively. Data were collected by the LSR Fortessa X-20 flow cytometer 491 and analyzed using the FlowJo-V10 software.

492

493 **ELISpot (Enzyme-Linked ImmunoSpot).** 96-well PVDF membrane plates were activated for 30 494 seconds with 70% ethanol, washed three times with PBS, and incubated with an anti-IFN-γ 495 antibody (7.5 µg/mL) for approximately 16 hours. After incubation, wells were washed three times 496 with PBS, blocked with 100 µL of media for 1 hour, and 100,000 tumor-infiltrating immune cells 497 were added in 100 µL of media. Cells were incubated for approximately 16 hours at 37°C and 5% 498 CO_2 while stimulated with PMA (0.02 µg/mL) and ionomycin (1 µg/mL). After incubation, plates 499 were washed eight times with PBS (200 µL per well) and incubated for 3 hours with an anti-IFN

500 γ antibody (1 µg/mL). Plates were washed eight times with PBS and wells incubated with 501 Streptavidin-Alkaline Phosphatase (diluted 1:1000) for 1.5 hours. Plates were washed eight times 502 with PBS and a chromogen substrate (Alkaline phosphatase conjugate substrate kit) was added 503 following manufacturer's instructions. The reaction was stopped after 45-60 minutes by washing 504 the plate with tap water. The plate was left to dry for at least 24 hours before counting spots on 505 an AID classic ELISpot reader (AID software, Autoimmun Diagnostika GmbH (AID), Strassberg, 506 Germany). Camera and counting settings were optimized and maintained for all samples. Data 507 were expressed as spots per million cells.

508

509 **ATP production in total leukocytes.** The ATP production by total tumor-infiltrating immune cells 510 was analyzed by bioluminescence using a commercial kit (Molecular Probes® ATP Determination 511 Kit), and the assay was performed according to the manufacturer's instructions.

512 **Immunoblotting.** The protein expression of total tumor-infiltrating leukocytes was evaluated by 513 Western Blotting. Initially, cells were mechanically disrupted in RIPA buffer, and further prepared 514 in Laemmli sample buffer. Samples were separated by molecular weight on a SDS-PAGE gel, 515 and proteins were then transferred to a nitrocellulose membrane. After blocking nonspecific 516 antigenic sites, the membranes were incubated overnight at 4°C with primary antibodies for Total 517 OXPHOS (1:500), PDH (Pyruvate Dehydrogenase E1-alpha subunit, 1:1000), and Mfn1 518 (Mitofusin 1, 1:1000). Secondary antibodies were incubated for 1 hour at room temperature 519 (IRDye 800 CW, LI-COR, 1:10,000). A list of the antibodies used can be found in the key 520 resources table. Immunodetection was performed using the fluorescence method (Odyssey FC

521 LI-COR, LI-COR Biosciences). Quantitative blot analyzes were performed using ImageJ.

522

523 **Quantitative Real-Time PCR.** Total RNA was extracted from frozen tumor samples using 524 TRIzol® reagent, according to the manufacturer's instructions. Isolated RNA was quantified using 525 a NanoDrop Spectrophotometer (NanoDrop Technologies, Rockland, DE) and denaturing 526 agarose gel electrophoresis was used to assess the quality of the samples. A conventional 527 reverse transcription reaction was performed to yield single-stranded cDNA. First strand cDNA 528 was synthesized from 1µg of total RNA using the High-Capacity cDNA Reverse Transcription Kit 529 according to the manufacturer's recommendations. The resulting cDNA was stored at −20 °C until 530 the expression analysis. The quantification of mRNA expression of genes was performed by RT 531 qPCR in a total volume of 10 µL, containing diluted cDNA template (1/10), forward and reverse 532 primers (200 nM each - ATG5, ATG7, BNIP3, LC3B, PARK2, PINK1, and ULK1), and SYBR 533 Green Master Mix. Primers sequences are described in **Table S1**. Gene expression was 534 performed using the 7500 Real Time PCR System (Applied Biosystems), following the universal 535 protocol of amplification: 95°C for 10 min, 40 cycles of 95°C for 15s, and 60°C for 1 min. 536 Dissociation curves were performed to test primers specificity. Relative gene expression 537 quantification was determined by $2^{-\Delta\Delta CT}$ method. Hprt1 was used as a reference gene.

538

Transmission Electron Microscopy (TEM). $CD8^+$ 539 T cells were first purified from tumors using 540 the EasySep™ Mouse CD8a Positive Selection Kit II according to the manufacturer's instructions. After that, the purified $CD8^+$ TILs (an average of $5x10^3$ 541 cells per sample) were pelleted and fixed 542 in 3.0% glutaraldehyde in 0.1M cacodylate buffer for 2 h at 4°C. The pellets were then rinsed in 543 buffer, post-fixed in 1.0% osmium tetroxide (OsO_4), and counterstained with aqueous 1% uranyl 544 acetate. The samples dehydration was performed in graded ethanol incubations, and then they 545 were embedded in standard Spurr resin. The resin embedded tissues were polymerized at 58°C

546 for 72 hours. Ultrathin sections were placed on grids, stained with lead citrate, and images were 547 collected using a transmission electron microscope TECNAI FEI G20 - 200 Kv. Mitochondrial 548 number, area, perimeter, and elongation were quantified by ImageJ (Scion Corporation, NIH, USA). Four samples/mice per group were analyzed, in which an average of ten $CD8^+$ 549 TILs were 550

identified (50 to 120 mitochondria analyzed per sample).

551

552 **In-silico analysis of a microarray dataset.** The enrichment plot for oxidative phosphorylation related genes was performed using the Gene Set Enrichment Analysis (GSEA)[59] 553 , comparing a 554 previously published microarray data from peripheral blood leukocytes in young endurance

athletes versus healthy controls (GEO database, Series GSE68072)[31] 555 .

556

557 **QUANTIFICATION AND STATISTICAL ANALYSIS**

558 **Statistical analysis.** Data are presented as mean ± standard error. Data normality was assessed 559 through Shapiro-Wilk's test. Comparisons for two groups were calculated using the unpaired 560 Student's *t* test. For more than two groups, comparisons were made by one-way ANOVA, followed 561 by Duncan's post hoc. Repeated measures data were analyzed by repeated measures ANOVA 562 or by fitting a mixed effects model. The software StatSoft Statistica 7 was used for the analysis. 563 The value of $p<0.05$ was used to determine statistical differences between groups.

564

565 **References**

566 1. Mariotto, A.B., Robin Yabroff, K., Shao, Y., Feuer, E.J., and Brown, M.L. (2011). 567 Projections of the cost of cancer care in the United States: 2010-2020. J. Natl. Cancer 568 Inst. 10.1093/jnci/djq495.

569 2. JEMAL, A., VINEIS, P., BRAY, F., TORRE, L., & FORMAN, D. (2019). THE CANCER 570 ATLAS Third. John M. Daniel, ed. (American Cancer Society).

571 3. Michna, L., Wagner, G.C., Lou, Y.R., Xie, J.G., Peng, Q.Y., Lin, Y., Carlson, K., Shih, 572 W.J., Conney, A.H., and Lu, Y.P. (2006). Inhibitory effects of voluntary running wheel 573 exercise on UVB-induced skin carcinogenesis in SKH-1 mice. Carcinogenesis *27*, 2108– 574 2115. 10.1093/carcin/bgl057.

575 4. Goh, J., Tsai, J., Bammler, T.K., Farin, F.M., Endicott, E., and Ladiges, W.C. (2013). 576 Exercise training in transgenic mice is associated with attenuation of early breast cancer 577 growth in a dose-dependent manner. PLoS One *8*, e80123.

578 10.1371/journal.pone.0080123.

579 5. Wolff, G., Balke, J.E., Andras, I.E., Park, M., and Toborek, M. (2014). Exercise modulates 580 redox-sensitive small GTPase activity in the brain microvasculature in a model of brain 581 metastasis formation. PLoS One *9*, 1–8. 10.1371/journal.pone.0097033. 582 6. Ju, J., Nolan, B., Cheh, M., Bose, M., Lin, Y., Wagner, G.C., and Yang, C.S. (2008). 583 Voluntary exercise inhibits intestinal tumorigenesis in Apc(Min/+) mice and 584 azoxymethane/dextran sulfate sodium-treated mice. BMC

Cancer *8*, 316. 10.1186/1471- 585 2407-8-316.
586 7. Roebuck, B.D., McCaffrey, J., and Baumgartner, K.J. (1990). Protective Effects of
587 Voluntary Exercise during the Postinitiation Phase of Pancreatic Carcinogenesis in the 588 Rat. Cancer Res. *50*, 6811–6816.
589 8. Hojman, P., Fjelbye, J., Zerahn, B., Christensen, J.F., Dethlefsen, C., Lonkvist, C.K., 590 Brandt, C., Gissel, H., Pedersen, B.K., and Gehl, J. (2014). Voluntary exercise prevents 591 cisplatin-induced muscle wasting during chemotherapy in mice. PLoS One *9*, e109030. 592 10.1371/journal.pone.0109030.
593 9. Betof, A.S., Lascola, C.D., Weitzel, D., Landon, C., Scarbrough, P.M., Devi, G.R., 594 Palmer, G., Jones, L.W., and Dewhirst, M.W. (2015). Modulation of murine breast tumor 595 vascularity, hypoxia and chemotherapeutic response by exercise. J. Natl. Cancer Inst. 596 *107*, 1–5. 10.1093/jnci/djv040.
597 10. Higgins, K.A., Park, D., Lee, G.Y., Curran, W.J., and Deng, X. (2014). Exercise-induced 598 lung cancer regression: Mechanistic findings from a mouse model. Cancer *120*, 3302– 599 3310. 10.1002/cncr.28878.

600 11. Moore, S.C., Lee, I.M., Weiderpass, E., Campbell, P.T., Sampson, J.N., Kitahara, C.M., 601 Keadle, S.K., Arem, H., De Gonzalez, A.B., Hartge, P., et al. (2016). Association of 602 leisure-time physical activity with risk of 26 types of cancer in 1.44 million adults. JAMA 603 Intern. Med. *176*, 816–825. 10.1001/jamainternmed.2016.1548.
604 12. Being inactive and cancer risk - World Cancer Research Fund https://www.wcrf 605 uk.org/preventing-cancer/what-can-increase-your-risk-of-cancer/being-inactive-and 606 cancer-risk/.
607 13. Koelwyn, G.J., Jones, L.W., and Moslehi, J. (2014). Unravelling the causes of reduced 608 peak oxygen consumption in patients with cancer: Complex, timely, and necessary. J. 609 Am. Coll. Cardiol. *64*, 1320–1322. 10.1016/j.jacc.2014.07.949.
610 14. Cramer, L., Hildebrandt, B., Kung, T., Wichmann, K., Springer, J., Doehner, W., Sandek, 611 A., Valentova, M., Stojakovic, T., Scharnagl, H., et al. (2014). Cardiovascular function and 612 predictors of exercise capacity in patients with colorectal cancer. J. Am. Coll. Cardiol. *64*, 613 1310–1319. 10.1016/j.jacc.2014.07.948.
614 15. Jones, L.W., Courneya, K.S., Mackey, J.R., Muss, H.B., Pituskin, E.N., Scott, J.M., 615 Hornsby, W.E., Coan, A.D., Herndon, J.E., Douglas, P.S., et al. (2012). Cardiopulmonary 616 function and age-related decline across the breast cancer: Survivorship continuum. J. 617 Clin. Oncol. *30*, 2530–2537. 10.1200/JCO.2011.39.9014.
618 16. Piercy, K.L., Troiano, R.P., Ballard, R.M., Carlson, S.A., Fulton, J.E., Galuska, D.A., 619 George, S.M., and Olson, R.D. (2018). The Physical Activity Guidelines for Americans. 620 JAMA *320*, 2020–2028. 10.1001/JAMA.2018.14854.
621 17. Emery, A., Moore, S., Turner, J.E., and Campbell, J.P. (2022). Reframing How Physical 622 Activity Reduces The Incidence of Clinically-Diagnosed Cancers: Appraising Exercise 623 Induced Immuno-Modulation As An Integral Mechanism. Front. Oncol. *12*. 624 10.3389/FONC.2022.788113.

625 18. Pedersen, L., Idorn, M., Olofsson, G.H., Lauenborg, B., Nookaew, I., Hansen, R.H., 626 Johannesen, H.H., Becker, J.C., Pedersen, K.S., Dethlefsen, C., et al. (2016). Voluntary 627 running suppresses tumor growth through epinephrine- and IL-6-dependent NK cell 628 mobilization and redistribution. Cell Metab. *23*, 554–562. 10.1016/j.cmet.2016.01.011. 629 19. Rundqvist, H., Velic, P., Barbieri, L., Gameiro, P.A., Bargiela, D., Gojkovic, M., Mijwel, S., 630 Reitzner, S.M., and Johnson, R. (2020). Cytotoxic T-cells mediate exercise- induced 631 reductions in tumor growth. 1–25.
632 20. Koelwyn, G.J., Zhuang, X., Tammela, T., Schietinger, A., and Jones, L.W. (2020). 633 Exercise and immunometabolic regulation in cancer. Nat. Metab. *2*, 849–857. 634 10.1038/s42255-020-00277-4.
635 21. Campbell, J.P., and Turner, J.E. (2018). Debunking the myth of exercise-induced immune 636 suppression: Redefining the impact of exercise on immunological health across the 637 lifespan. Front. Immunol. *9*, 648. 10.3389/FIMMU.2018.00648/BIBTEX.
638 22. Gomes-Santos, I.L., Amoozgar, Z., Kumar, A.S., Ho, W.W., Roh, K., Talele, N.P., Curtis, 639 H., Kawaguchi, K., Jain, R.K., and Fukumura, D. (2021). Exercise Training Improves 640 Tumor Control by Increasing CD8+ T-cell Infiltration via CXCR3 Signaling and Sensitizes 641 Breast Cancer to Immune Checkpoint Blockade. Cancer Immunol. Res. *9*, 765–778. 642 10.1158/2326-6066.CIR-20-0499.
643 23. Buck, M.D.D., O'Sullivan, D., Klein Geltink, R.I.I., Curtis, J.D.D., Chang, C.H., Sanin, 644 D.E.E., Qiu, J., Kretz, O., Braas, D., van der Windt, G.J.J.W., et al. (2016). Mitochondrial 645 Dynamics Controls T Cell Fate through Metabolic Programming. Cell *166*, 63–76. 646 10.1016/j.cell.2016.05.035.
647 24. Scharping, N.E., Menk, A. V., Moreci, R.S., Whetstone, R.D., Dadey, R.E., Watkins, S.C., 648 Ferris, R.L., and Delgoffe, G.M. (2016). The Tumor Microenvironment Represses T Cell 649 Mitochondrial Biogenesis to Drive Intratumoral T Cell Metabolic Insufficiency and 650 Dysfunction. Immunity *45*, 374–388. 10.1016/j.immuni.2016.07.009.

651 25. Yu, Y.R., Imrichova, H., Wang, H., Chao, T., Xiao, Z., Gao, M., Rincon-Restrepo, M., 652 Franco, F., Genolet, R., Cheng, W.C., et al. (2020). Disturbed mitochondrial dynamics in 653 CD8+ TILs reinforce T cell exhaustion. Nat. Immunol. 10.1038/s41590-020-0793-3. 654 26. Egan, B., and Zierath, J.R. (2013). Exercise metabolism and the molecular regulation of 655 skeletal muscle adaptation. Cell Metab. *17*, 162–184. 10.1016/j.cmet.2012.12.012. 656 27. Singer, M., Wang, C., Cong, L., Marjanovic, N.D., Kowalczyk, M.S., Zhang, H., Nyman, 657 J., Sakuishi, K., Kurtulus, S., Gennert, D., et al. (2016). A Distinct Gene Module for 658 Dysfunction Uncoupled from Activation in Tumor-Infiltrating T Cells. Cell *166*, 1500- 659 1511.e9. 10.1016/j.cell.2016.08.052.
660 28. Sidarala, V., Zhu, J., Levi-D'Ancona, E., Pearson, G.L., Reck, E.C., Walker, E.M., 661 Kaufman, B.A., and Soleimanpour, S.A. (2022). Mitofusin 1 and 2 regulation of 662 mitochondrial DNA content is a critical determinant of glucose homeostasis. Nat. 663 Commun. 2022 131 *13*, 1–16. 10.1038/s41467-022-29945-7.
664 29. Zhang, J. (2013). Autophagy and mitophagy in cellular damage control. Redox Biol. *1*, 19. 665 10.1016/J.REDOX.2012.11.008.

666 30. Lee, S., Son, J.Y., Lee, J., and Cheong, H. (2023). Unraveling the Intricacies of 667 Autophagy and Mitophagy: Implications in Cancer Biology. Cells 2023, Vol. 12, Page 668 2742 *12*, 2742. 10.3390/CELLS12232742.
669 31. Liu, D., Wang, R., Grant, A.R., Zhang, J., Gordon, P.M., Wei, Y., and Chen, P. (2017). 670 Immune adaptation to chronic intense exercise training: new microarray evidence. BMC 671 Genomics *18*, 29. 10.1186/s12864-016-3388-5.
672 32. Schadler, K.L., Thomas, N.J., Galie, P.A., Bhang, D.H., Roby, K.C., Addai, P., Till, J.E., 673 Sturgeon, K., Zaslavsky, A., Chen, C.S., et al. (2016). Tumor vessel normalization after 674 aerobic exercise enhances chemotherapeutic efficacy. Oncotarget *7*, 65429–65440. 675 10.18632/oncotarget.11748.
676 33. Kruijsen-Jaarsma, M., Révész, D., Bierings, M.B., Buffart, L.M., and Takken, T. (2013). 677 Effects of exercise on immune function in patients with cancer: A systematic review. 678 Exerc. Immunol. Rev. *19*, 120–143.
679 34. Koelwyn, G.J., Quail, D.F., Zhang, X., White, R.M., and Jones, L.W. (2017). Exercise 680 dependent regulation of the tumour microenvironment. Nat. Rev. Cancer *17*, 545–549. 681 10.1038/nrc.2017.78.
682 35. Lakoski, S.G., Willis, B.L., Barlow, C.E., Leonard, D., Gao, A., Radford, N.B., Farrell, 683 S.W., Douglas, P.S., Berry, J.D., Defina, L.F., et al. (2015). Midlife cardiorespiratory 684 fitness, incident cancer, and survival after cancer in men: The Cooper Center 685 Longitudinal Study. JAMA Oncol. *1*, 231–237. 10.1001/jamaoncol.2015.0226. 686 36. Bonetto, A., Rupert, J.E., Barreto, R., and Zimmers, T.A. (2016). The Colon-26 687 Carcinoma Tumor-bearing Mouse as a Model for the Study of Cancer Cachexia. J. Vis. 688 Exp., 54893. 10.3791/54893.
689 37. Bonetto, A., Kays, J.K., Parker, V.A., Matthews, R.R., Barreto, R., Puppa, M.J., Kang, 690 K.S., Carson, J.A., Guise, T.A., Mohammad, K.S., et al. (2017). Differential bone loss in 691 mouse models of colon cancer cachexia. Front. Physiol. *7*. 10.3389/fphys.2016.00679. 692 38. Ballarò, R., Beltrà, M., De Lucia, S., Pin, F., Ranjbar, K., Hulmi, J.J., Costelli, P., and 693 Penna, F. (2019). Moderate exercise in mice improves cancer plus chemotherapy 694 induced muscle wasting and mitochondrial alterations. FASEB J. *33*, 5482–5494. 695 10.1096/FJ.201801862R.
696 39. Wenes, M., Shang, M., Di Matteo, M., Goveia, J., Martín-Pérez, R., Serneels, J., Prenen, 697 H., Ghesquière, B., Carmeliet, P., and Mazzone, M. (2016). Macrophage Metabolism 698 Controls Tumor Blood Vessel Morphogenesis and Metastasis. Cell Metab. *24*, 701–715. 699 10.1016/j.cmet.2016.09.008.
700 40. Palazon, A., Tyrakis, P.A., Macias, D., Veliça, P., Rundqvist, H., Fitzpatrick, S., Vojnovic, 701 N., Phan, A.T., Loman, N., Hedenfalk, I., et al. (2017). An HIF-1α/VEGF-A Axis in

702 Cytotoxic T Cells Regulates Tumor Progression. Cancer Cell *32*, 669-683.e5. 703 10.1016/j.ccell.2017.10.003.
704 41. EA, R., J, E., and BL, H. (2015). Stress, metabolism and cancer: integrated pathways 705 contributing to immune suppression. Cancer J. *21*, 97–103.
706 10.1097/PPO.0000000000000107.

707 42. Togashi, Y., Shitara, K., and Nishikawa, H. (2019). Regulatory T cells in cancer 708 immunosuppression — implications for anticancer therapy at Nature Publishing Group, 709 10.1038/s41571-019-0175-7 10.1038/s41571-019-0175-7.
710 43. Desdín-Micó, G., Soto-Heredero, G., and Mittelbrunn, M. (2018). Mitochondrial activity in 711 T cells at Elsevier B.V., 10.1016/j.mito.2017.10.006 10.1016/j.mito.2017.10.006. 712 44. Martínez-Reyes, I., and Chandel, N.S. (2020). Mitochondrial TCA cycle metabolites 713 control physiology and disease, 10.1038/s41467-019-13668-3 10.1038/s41467-019- 714 13668-3.
715 45. Franco, F., Jaccard, A., Romero, P., Yu, Y.R., and Ho, P.C. (2020). Metabolic and 716 epigenetic regulation of T-cell exhaustion. Nat. Metab. *2*, 1001–1012. 10.1038/s42255- 717 020-00280-9.
718 46. Michalek, R.D., Gerriets, V.A., Jacobs, S.R., Macintyre, A.N., MacIver, N.J., Mason, E.F., 719 Sullivan, S.A., Nichols, A.G., and Rathmell, J.C. (2011). Cutting Edge: Distinct Glycolytic 720 and Lipid Oxidative Metabolic Programs Are Essential for Effector and Regulatory CD4 + 721 T Cell Subsets . J. Immunol. *186*, 3299–3303. 10.4049/jimmunol.1003613.
722 47. Tan, H., Yang, K., Li, Y., Shaw, T.I., Wang, Y., Blanco, D.B., Wang, X., Cho, J.H., Wang, 723 H., Rankin, S., et al. (2017). Integrative Proteomics and Phosphoproteomics Profiling 724 Reveals Dynamic Signaling Networks and Bioenergetics Pathways Underlying T Cell 725 Activation. Immunity *46*, 488–503. 10.1016/j.immuni.2017.02.010. 726 48. Diebold, L., and Chandel, N.S. (2016). Mitochondrial ROS regulation of proliferating cells 727 at Elsevier Inc., 10.1016/j.freeradbiomed.2016.04.198
728 10.1016/j.freeradbiomed.2016.04.198.
729 49. Dowling, R.J.O., Goodwin, P.J., and Stambolic, V. (2011). Understanding the benefit of 730 metformin use in cancer treatment. BMC Med. *9*, 1–6. 10.1186/1741-7015-9- 731 33/COMMENTS.
732 50. Yu, H., Zhong, X., Gao, P., Shi, J., Wu, Z., Guo, Z., Wang, Z., and Song, Y. (2019). The 733 Potential Effect of Metformin on Cancer: An Umbrella Review. Front. Endocrinol. 734 (Lausanne). *10*. 10.3389/FENDO.2019.00617.
735 51. Laker, R.C., Drake, J.C., Wilson, R.J., Lira, V.A., Lewellen, B.M., Ryall, K.A., Fisher, 736 C.C., Zhang, M., Saucerman, J.J., Goodyear, L.J., et al. (2017). Ampk phosphorylation of 737 Ulk1 is required for targeting of mitochondria to lysosomes in exercise-induced 738 mitophagy. Nat. Commun. 2017 81 *8*, 1–13. 10.1038/s41467-017-00520-9. 739 52. Fan, W., and Evans, R.M. (2017). Exercise Mimetics: Impact on Health and Performance.
740 Cell Metab. *25*, 242. 10.1016/J.CMET.2016.10.022.
741 53. Gubert, C., and Hannan, A.J. (2021). Exercise mimetics: harnessing the therapeutic 742 effects of physical activity. Nat. Rev. Drug Discov. 2021 2011 *20*, 862–879. 743 10.1038/s41573-021-00217-1.
744 54. Huang, Q., Wu, M., Wu, X., Zhang, Y., and Xia, Y. (2022). Muscle-to-tumor crosstalk: The 745 effect of exercise-induced myokine on cancer progression. Biochim. Biophys. Acta - Rev. 746 Cancer *1877*, 188761. 10.1016/J.BBCAN.2022.188761.
747 55. Gebhardt, K., and Krüger, K. (2022). Supporting tumor therapy by exercise: boosting T 748 cell immunity by myokines. Signal Transduct. Target. Ther. 2022 71 *7*, 1–2. 749 10.1038/s41392-022-01116-6.
750 56. Hojman, P., Gehl, J., Christensen, J.F., and Pedersen, B.K. (2018). Molecular 751 Mechanisms Linking Exercise to Cancer Prevention and Treatment. Cell Metab. *27*, 10– 752 21. 10.1016/j.cmet.2017.09.015.

753 57. Ferreira, J.C.B., Rolim, N.P.L., Bartholomeu, J.B., Gobatto, C.A., Kokubun, E., and Brum, 754 P.C. (2007). Maximal lactate steady state in running mice: Effect of exercise training. 755 Clin. Exp. Pharmacol. Physiol. 10.1111/j.1440-1681.2007.04635.x. 756 58. Chang, C.H., Curtis, J.D., Maggi, L.B., Faubert, B., Villarino, A. V., O'Sullivan, D., Huang, 757 S.C.C., Van Der Windt, G.J.W., Blagih, J., Qiu, J., et al. (2013). XPosttranscriptional 758 control of T cell effector function by aerobic glycolysis. Cell *153*, 1239–1251. 759 10.1016/j.cell.2013.05.016.
760 59. Subramanian, A., Tamayo, P., Mootha, V.K., Mukherjee, S., Ebert, B.L., Gillette, M.A., 761 Paulovich, A., Pomeroy, S.L., Golub, T.R., Lander, E.S., et al. (2005). Gene set 762 enrichment analysis: A knowledge-based approach for interpreting genome-wide 763 expression profiles. Proc. Natl. Acad. Sci. U. S. A. *102*, 15545–15550. 764 10.1073/PNAS.0506580102/SUPPL_FILE/06580FIG7.JPG.
765

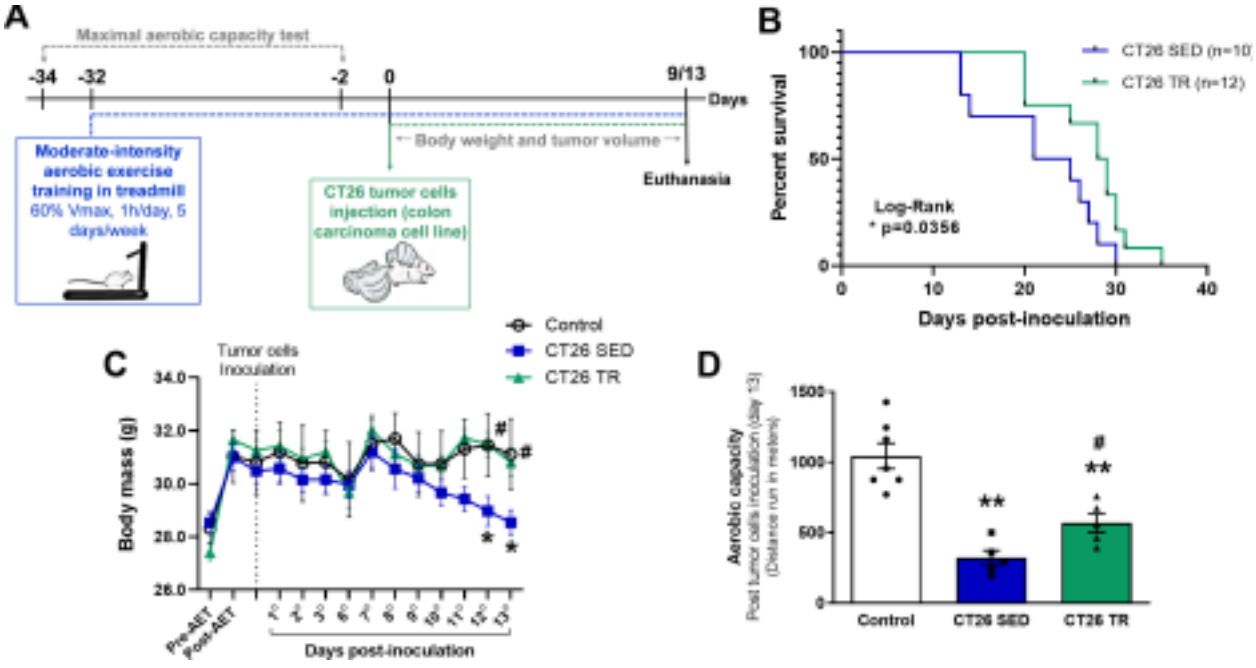

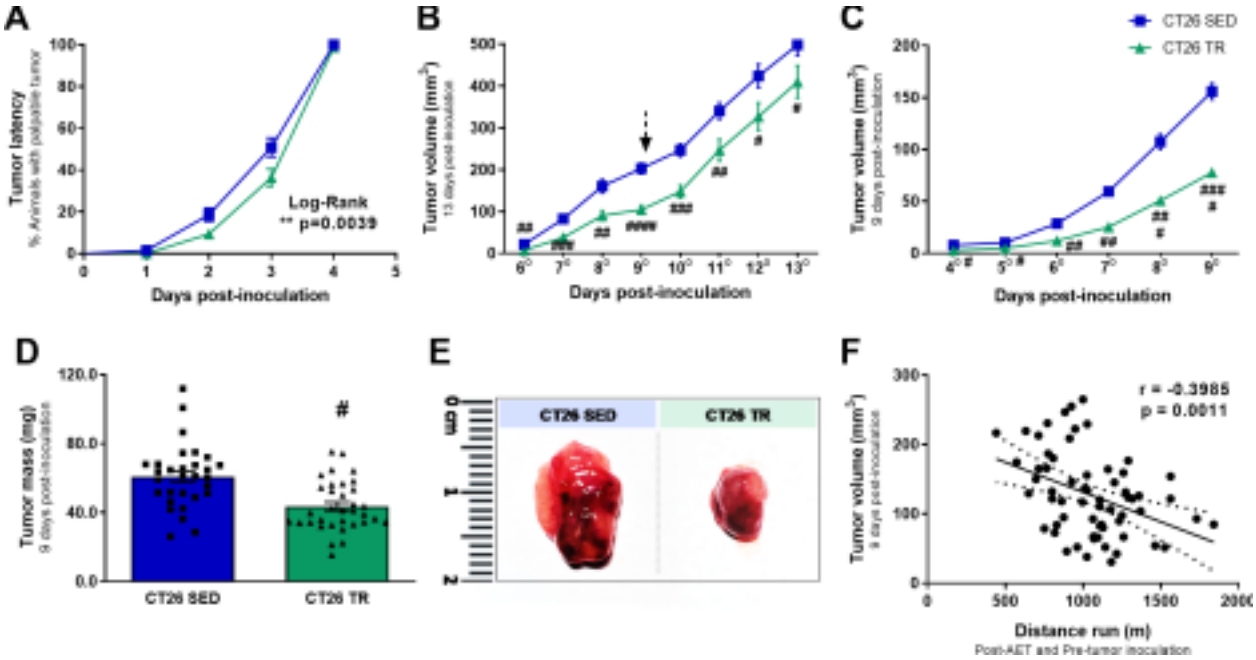

Journal Pre-proof

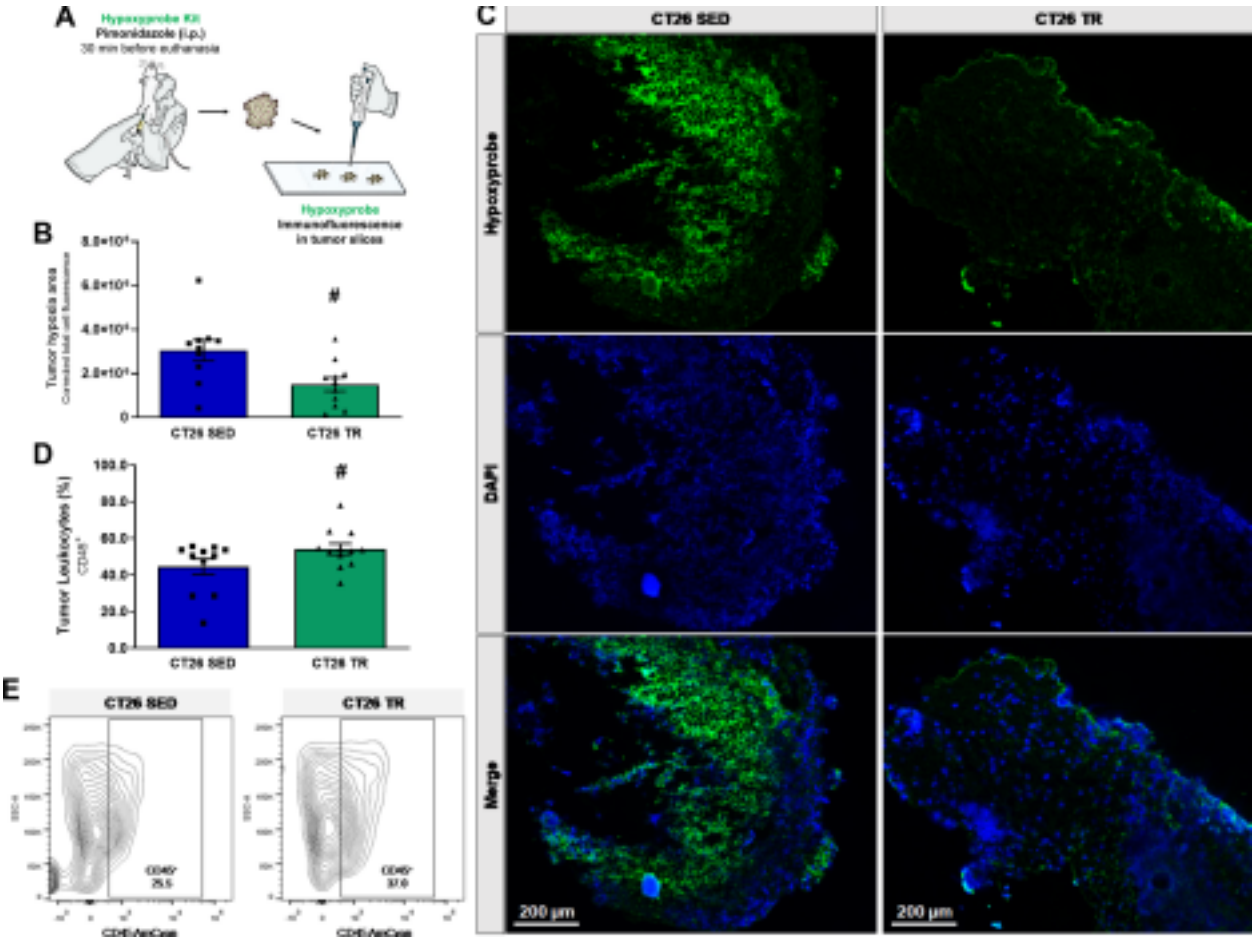

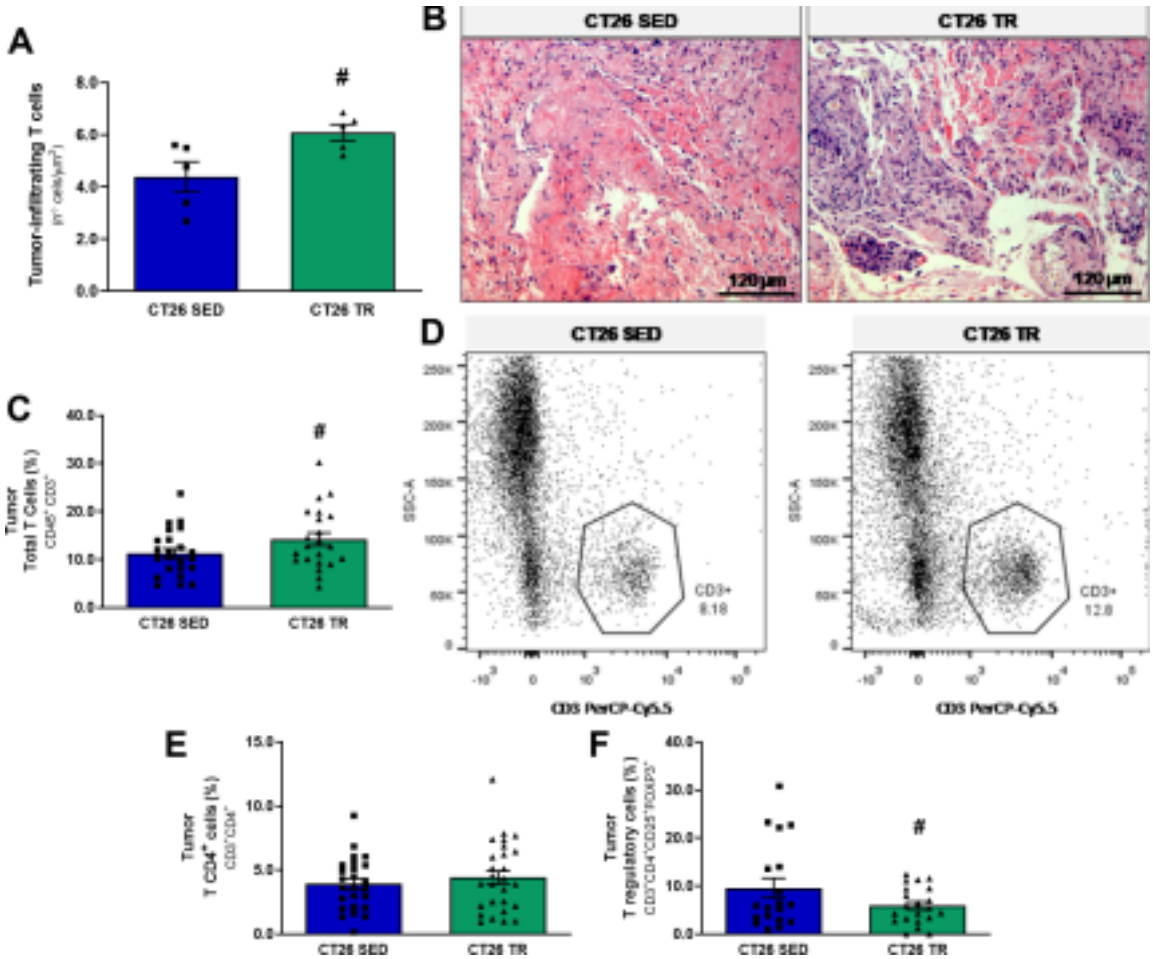

Journal Pre-proof

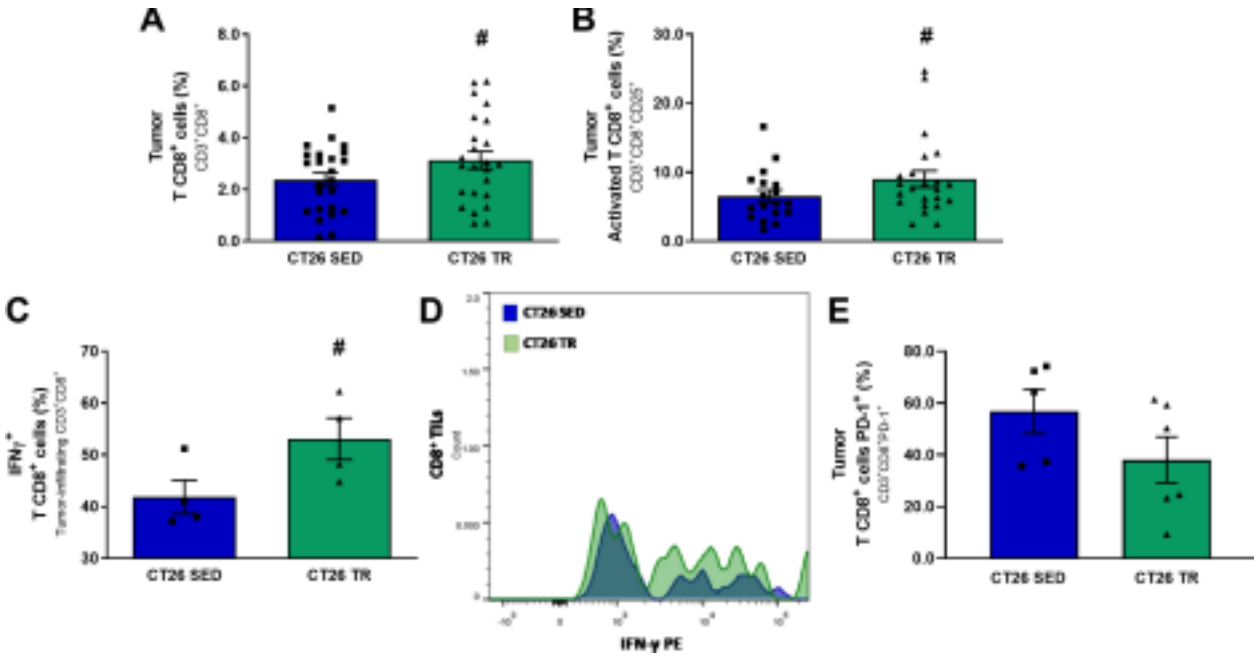

Journal Pre-proof

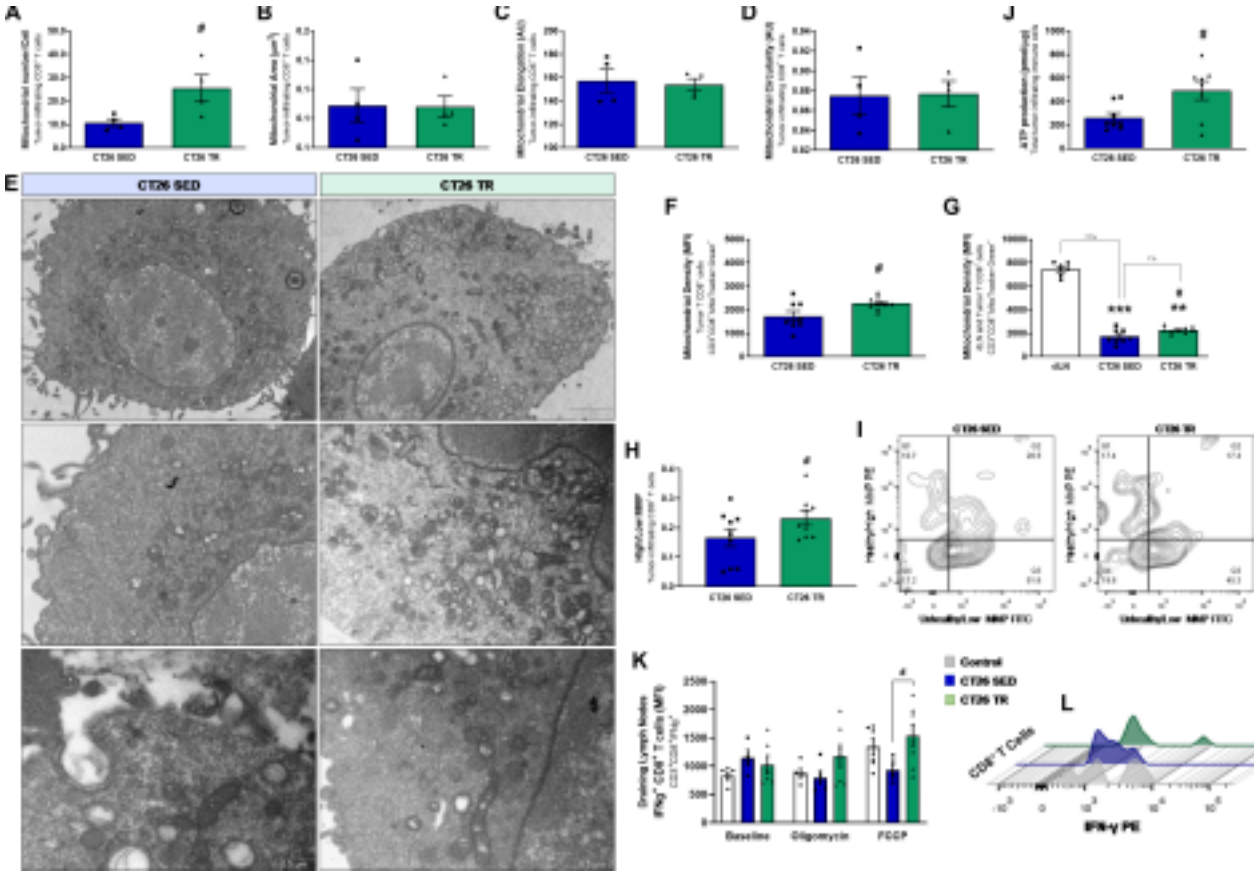

HIGHLIGHTS

Exercise training reduces tumor growth and improves survival in colorectal cancer.

Trained mice present tumors with less hypoxia and higher $CD8^+$ T cells infiltration.

The production of IFNɣ by $CD8^+$ TIL is increased in exercise-trained mice. $CD8^+$

TIL from trained mice show higher mitochondrial density and function.

KEY RESOURCES TABLE

REAGENT or RESOURCE	SOURCE	IDENTIFIER
Antibodies		
Total OXPHOS Rodent WB Antibody Cocktail	Abcam	Cat# ab110413; RRID:AB_2629281
Mouse monoclonal Pyruvate Dehydrogenase E1-alpha subunit [8D10E6]	Abcam	Cat# ab110334; RRID:AB_10866116
Mouse monoclonal Anti-Mitofusin 1 [11E91H12]	Abcam	Cat# ab126575, RRID:AB_11141234
IRDye® 800CW Goat anti-Mouse IgG Secondary Antibody	LI-COR Biosciences	Cat# 926-32210; RRID:AB_621842
Goat anti-Rat IgG (H+L) Cross-Adsorbed Secondary Antibody, Alexa Fluor™ 488	Thermo Fisher Scientific	Cat# A-11006; RRID:AB_2534074
Rat Anti-Mouse IFN-g (Interferon-gamma) Monoclonal Antibody, Unconjugated, Clone AN18	MABTECH	Cat# 3321-3-250; RRID:AB_907279
Fixable Viability Stain 575V	BD Biosciences	Cat# 565694; RRID:AB_2869702
TruStain FcX™ (anti-mouse CD16/32) Antibody	BioLegend	Cat# 101319; RRID:AB_1574975

Brilliant Violet 510™ anti-mouse CD45	BioLegend	Cat# 103138; RRID:AB_2561392
Armenian Hamster Anti-CD3e, PerCP-Cy5.5 Conjugated, Clone 145-2C11	BD Biosciences	Cat# 551163, RRID:AB_394082
Rat Anti-Mouse CD4, APC-H7 Conjugated, Clone GK1.5	BD Biosciences	Cat# 560181; RRID:AB_1645235
Rat Anti-CD8a, PE-Cy7 Conjugated, Clone 53-6.7	BD Biosciences	Cat# 552877; RRID:AB_394506
Anti-CD25 (PC61.5), eFluor™ 450, eBioscience	Thermo Fisher Scientific	Cat# 48-0251-82; RRID:AB_10671 550
Rat Anti-Mouse Foxp3, PE Conjugated	BD Biosciences	Cat# 560414; RRID:AB_1645252

Brilliant Violet 421™ anti-mouse CD279 (PD-1) O	BioLegend	Cat# 135221; RRID:AB_2561447
PE anti-mouse IFN-gamma J	BioLegend	Cat# 505807; RRID:AB_315402
Bacterial and virus strains		
Biological samples		
Chemicals, peptides, and recombinant proteins		
Collagenase, Type IV, powder	Thermo Fisher Scientific	Cat# 17104019
Deoxyribonuclease I from bovine pancreas	Sigma-Aldrich	Cat# D5025-15KU
Percoll density gradient media	Cytiva	Cat# 17089101
Tissue-Tek® O.C.T. Compound	Sakura Finetek	Cat# 4583
RPMI 1640 Medium	Gibco™	Cat# 11875093
Fetal Bovine Serum	Gibco™	Cat# A5256701
Penicillin-Streptomycin	Sigma-Aldrich	Cat# P4333

PBS, pH 7.4	Gibco™	Cat# 10010023
Phorbol 12-myristate 13-acetate	Sigma-Aldrich	Cat# P8139
Ionomycin calcium salt from Streptomyces conglobatus	Sigma-Aldrich	Cat# 56092-82-1
MitoTracker™ Green FM Dye, for flow cytometry	Thermo Fisher Scientific	Cat# M46750

TRIzol™ Reagent	Thermo Fisher Scientific	Cat# 15596018
ELISpot conjugate: Streptavidin-ALP	MABTECH	Cat# 3310-10-1000
Mounting Medium With DAPI - Aqueous, Fluoroshield	Abcam	Cat# ab104139
Critical commercial assays		
High-Capacity cDNA Reverse Transcription Kit	Applied Biosystems™	Cat# 4368814
PowerUp SYBR Green Master Mix for qPCR	Applied Biosystems	Cat# A25776
Hypoxyprobe Kit	Hypoxyprobe, Inc	Cat# HP1-1000Kit
BD Cytofix/Cytoperm™ Plus Fixation/Permeabilization Solution Kit with BD GolgiStop™	BD Biosciences	Cat# 554715
JC-1 Mitochondrial Membrane Potential Flow Cytometry Assay Kit	Cayman Chemical	Cat# 701560
AP Conjugate Substrate Kit	Bio-Rad	Cat# 1706432
Molecular Probes™ ATP Determination Kit	Thermo Fisher Scientific	Cat# A22066

EasySep™ Mouse CD8a Positive Selection Kit II P	STEMCELL Technologies	Cat# 18953
BD Pharmingen™ Mouse Foxp3 Buffer Set I	BD Biosciences	Cat# 560409
Deposited data a		
Microarrays data urn	Liu D. et al, 2017 - NCBI PMID: 28056786	NCBI GEO: GSE68072
Data sets jo	Mendeley Data, Voltarelli, Vanessa (2024)	doi:10.17632/wb734 hz2wc.1
Experimental models: Cell lines		
CT26.WT	ATCC®	CRL-2638; RRID:CVCL_7256
Experimental models: Organisms/strains		

Balb/c mice	ANILAB, Brazil	www.anilab.com.br
Oligonucleotides		
Primers for ATG5, ATG7, BNIP3, LC3B, HPRT1, PARK2, PINK1, ULK1, see Table S1	This paper	N/A
Recombinant DNA		
Software and algorithms		

GraphPad Prism 8	GraphPad Software	RRID:SCR_002798; http://www.graphpad .com/
FlowJo-V10	FlowJoSoftware	RRID:SCR_008520; https://www.flowjo.co m/solutions/flowjo
ImageJ	NIH	RRID:SCR_003070; https://imagej.net/
StatSoft Statistica 7	StatSoft	RRID:SCR_014213; http://www.statsoft .c om/Products/STATI STICA/Product-Index
BioRender	BioRender	RRID:SCR_018361; http://biorender.com

Other		

Journal Pre-p